CONVECTION PATTERN MORPHOLOGY AND VARIATIONS
(Invited Review)

R. A. Heelis
Center for Space Science
P.O. Box 688
The University of Texas at Dallas
Richardson, TX 75080

A fairly straightforward consideration of the interaction between a southward interplanetary magnetic field and the earth's magnetic field will result in the prediction of a two-cell convection pattern in the high latitude ionosphere. This is shown schematically in Figure 1 where the antisunward flow at high latitudes results from the application of the solar wind electric field to the ionoshpere and the return sunward flow results from an electric field generated in the plasma sheet to ensure continuity.

This convection pattern can be quite easily characterized in terms of the radius of the approximately circular region containing the anti-sunward flow, called the polar cap and the maximum potential difference applied across this region. The polar cap potential difference can be shown to be a sensitive function of the orientation of the interplanetary magnetic field and consideration of magnetic flux conservation can predict a dependence of the polar cap radius on the polar cap potential (Siscoe, 1982). The size of the polar cap is predicted to vary as the 3/16 power of the potential difference. This dependence is not strong enough to be unequivocably demonstrated by the data. However, Figure 2 shows the dependence of the polar cap potential drop on the ratio of electric fields inside and outside the merging region (Reiff et al., 1981). Merging theory simply expresses this ratio as the cosine of the angle between the IMF and a plane perpendicular to the sun-earth line (i.e. Bz/Bx) (Hill, 1974).

It can be seen from Figure 2 that the polar cap potential increases as the IMF becomes more southward and that a relatively large potential drop remains even when the IMF turns northward. This residual potential drop has been attributed to a 'viscous interaction' process at the flanks of the magnetosphere that exists in addition to the dayside merging process that operates when the IMF has a southward component. A more detailed analysis of the behavior of the potential difference when the IMF turns northward is shown in Figure 3 (Wygant et al., 1983). It displays an almost exponential decay, requiring some 2-4 hours to reach a residual value near 15 Kv.

In addition to a variation in the polar cap potential drop as a function of the IMF orientation examination of the signatures of ionospheric convection from satellites show that the cell geometry or cell shape is also dependent on the IMF. First observations of the flow geometry near local noon showed that substantial east-west flows could occur in this region. An arbitrary inspection of the data also showed that this flow could be predominantly to the east or predominantly to the west. Examples of these differing flow signatures are shown for almost identical orbital conditions in Figures 4 and 5. A compilation of such data without strict consideration of the IMF orientation leads to the concept of a restricted region of sunward flow near local noon sometimes called the 'throat'. Figure 6 shows a schematic of such a flow geometry generated from a mathematical model. Studies of the electric field near the dawn and dusk convection reversals had

already revealed a dependence of electric field magnitude on the IMF (Heppner, 1972). It was known that the antisunward flow on the poleward side of the convection reversal was larger on the dusk (dawn) side than on dawn (dusk) side if the IMF By component was negative (positive).

A rotation of the throat region was postulated to account for the previously known dependence of the dawn/dusk flow speeds on the IMF but it was recognized that the data base of convection signatures should be examined for different IMF orientations and that even then the single cuts available from satellites like AE and DE could not define the entire high latitude convection geometry. Examination of the AE data base shows that reproducible signatures of the convection pattern can be obtained if we restrict our attention to times when the IMF has a southward component ($Bz < 0$) and a normal garden hose orientation ($BxBy < 0$). Under these conditions the pattern can be generally characterized by dividing it into signatures seen when By is positive and when By is negative.

Figure 7 shows examples of the signature seen in the northern high latitude ionosphere when By is positive (and Bx is negative). The most reproducible feature is that the flow near local noon is directed toward dawn at all invariant latitudes between 70 and 80 degrees. If we trace the position of the zero potential line that separates cells in which the flow is either clockwise around the dawn side or anti-clockwise around the dusk side, we note that it shows a tendency to be displaced slightly to the dawn side of local noon. This results in the dusk convection cell being relatively large and almost circular in shape while the dawn cell is apparently more cresent shaped and abuts the dusk cell. A more detailed description of the convection geometry for this orientation of the IMF has been obtained by using simultaneous data from the DE satellite and ground based radars at Chatanika and Millstone Hill. This data set provides multiple data points around the high latitude region at which the electrostatic potential and flow direction are specified. The results of an examination of this data set are shown in Figure 8 and confirm our expectations.

Figure 9 shows examples of the northern hemisphere high latitude convection signature seen when the IMF By is negative (and Bx is positive). Contrasting these signatures with those shown in the previous two figures it can be seen that the flow with an anti-sunward component near local noon is directed toward dusk rather than toward dawn. In extreme cases when the magnitude of By greatly exceeds Bx the flow may be directed eastward as shown in the last two examples. In all cases however the flow signature is consistent with a more circular perimeter to the dawn cell with a cresent shaped dusk cell that surrounds it. To my knowledge a study of multipoint measurements to confirm such a flow geometry has not yet been completed. Figure 10 shows schematically the dayside high latitude flow geometry that exists in the northern hemisphere for different configurations of a southward IMF.

When the IMF has a northward component ($Bz > 0$) the observed convection velocities are usually much more structured both in the summer and in the winter hemispheres. Nevertheless large scale convection signatures can often be recognized and reproducible features emerge with a dependence on the IMF orientation. Figure 11 shows the most easily identified feature from S3-2 electric field data (Burke et al., 1982). Here sunward convection exists at the very highest magnetic latitudes where anti-sunward convection would normally be expected if the IMF had a southward component. Figure 12 shows the ion convection signature observed by DE-B during times of northward IMF. Similar regions of sunward convection are seen in this data base but additional features dependent on By can also be identified. Regions of anti-sunward convection on one or both sides of this high latitude sunward convection allow the identification of one and sometimes two convection cells within a region that can be associated with open field lines. These convection cells are labelled I and II in the figure. In addition to the convection cells within the polar cap there usually exists additional convection cells at lower latitudes that circulate in the same sense as the cells existing during times of southward IMF. These cells are labelled III and IV in the figure.

Examination of a large data base shows a dependence of the number of convection cells and their sense of circulation on the By component of the IMF. Figure 13 shows schematically these dependences for the high latitude northern hemisphere. When By is close to zero two convection cells apparently exist within the polar cap. They occupy the dawn and dusk sides and circulate anti-clockwise and clockwise respectively to produce sunward flow at the highest latitudes. At lower latitudes cresent shaped cells form about each of the polar cap cells and circulate in the manner expected for a southward IMF. When By is negative the dawn-side polar cap convection cell tends to disappear giving way to a slightly larger dusk-side cell and more turbulent flow on its dawn side. The two lower latitude convection cells remain. When By is positive the polar cap dawn-side cell remains and perhaps expands and more turbulent flow exists on its dusk side. Again the lower latitude convection cells remain. The completeness of the convection cells is extremely difficult to observe since the nightside high latitude convection is extremely turbulent during times of northward IMF. The convection pattern I have described is at least understandable in terms of solar-wind/magnetosphere interaction in which open field lines are recirculated in the polar cap and a viscous interaction process exists near the flanks of the magnetosphere's equatorial plane giving rise to the lower latitude convection cells.

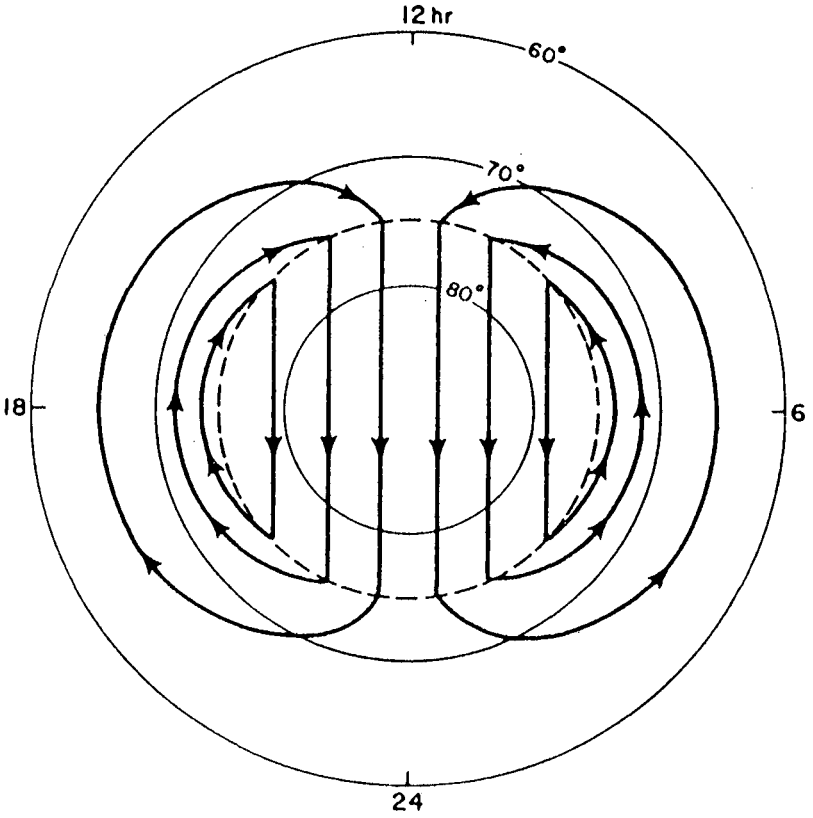

Figure 1.

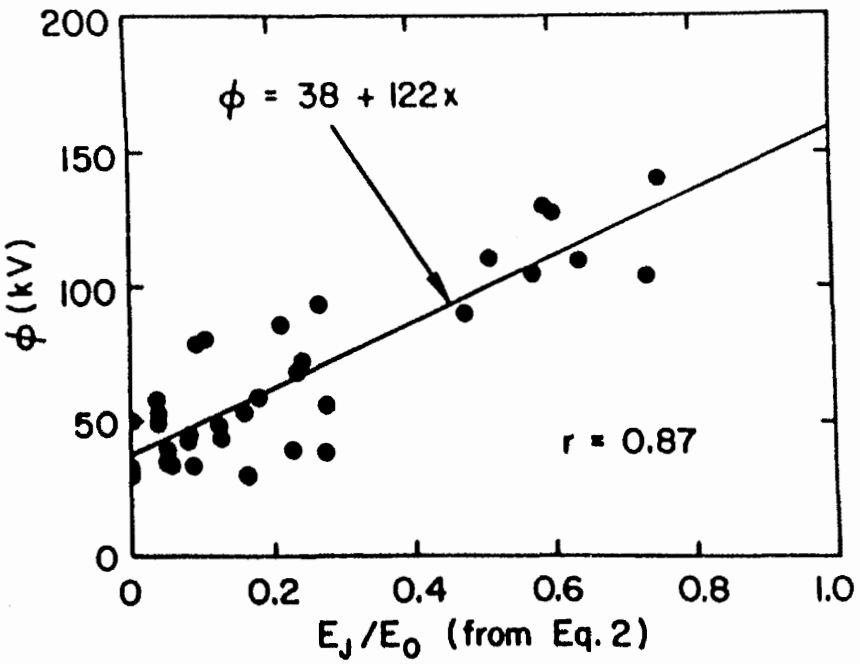

Figure 2.

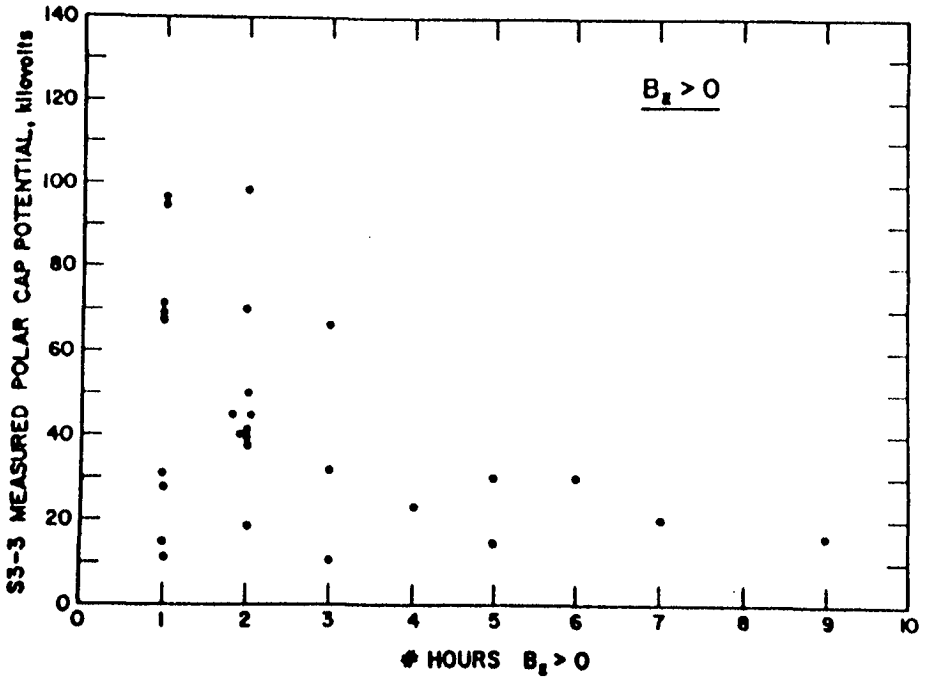
S3-3 MEASURED POLAR CAP POTENTIAL, kilovolts
140
120
100
80
60
40
20
0
0
1
2
3
4
5
6
7
8
9
10
$B_z > 0$
HOURS $B_z > 0$

Figure 3.

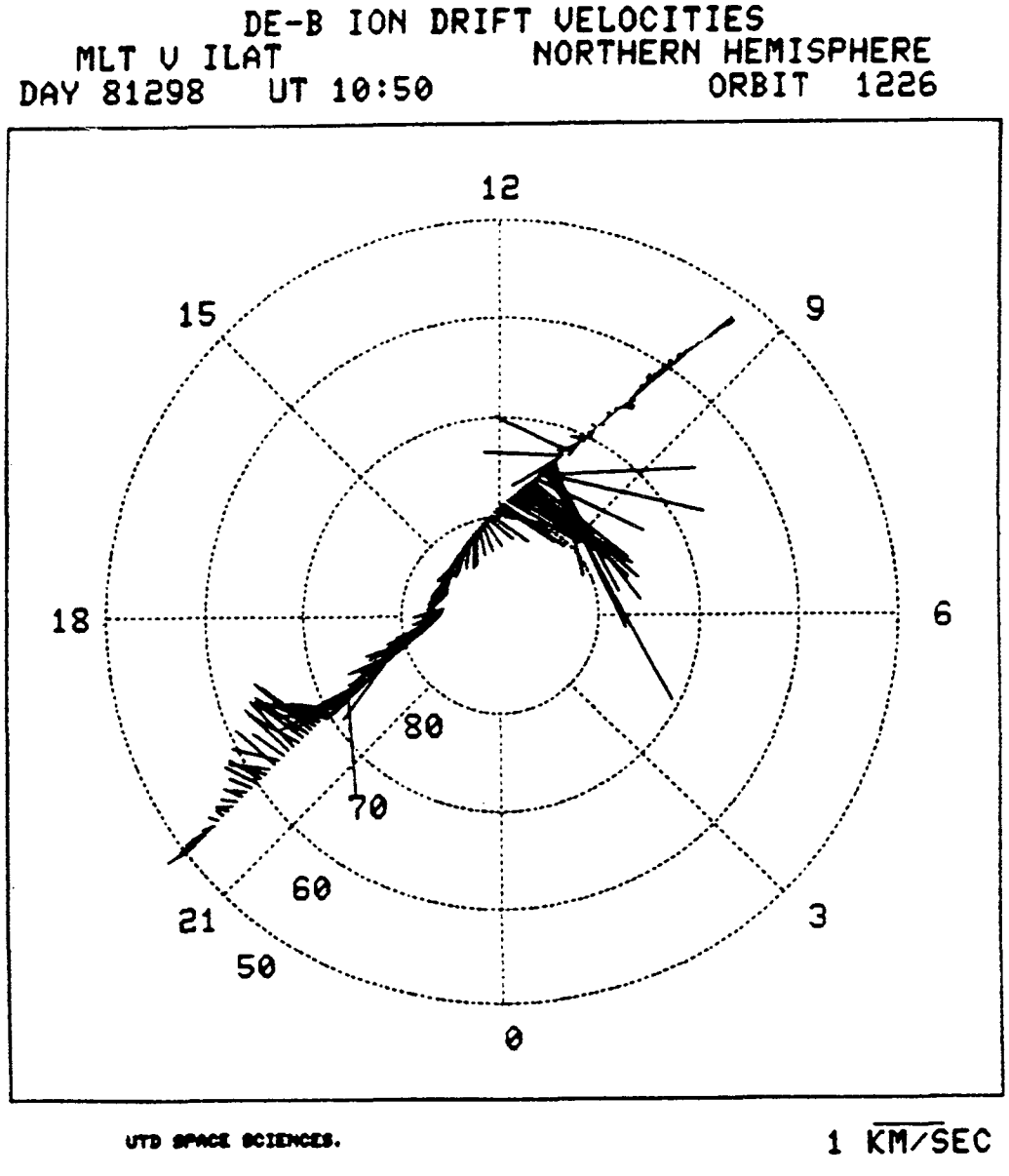
DE-B ION DRIFT VELOCITIES
MLT V ILAT
NORTHERN HEMISPHERE
DAY 81298 UT 10:50
ORBIT 1226
12
15
9
18
6
80
70
60
21
3
50
0
UTD SPACE SCIENCES.
1 KM/SEC

Figure 4.

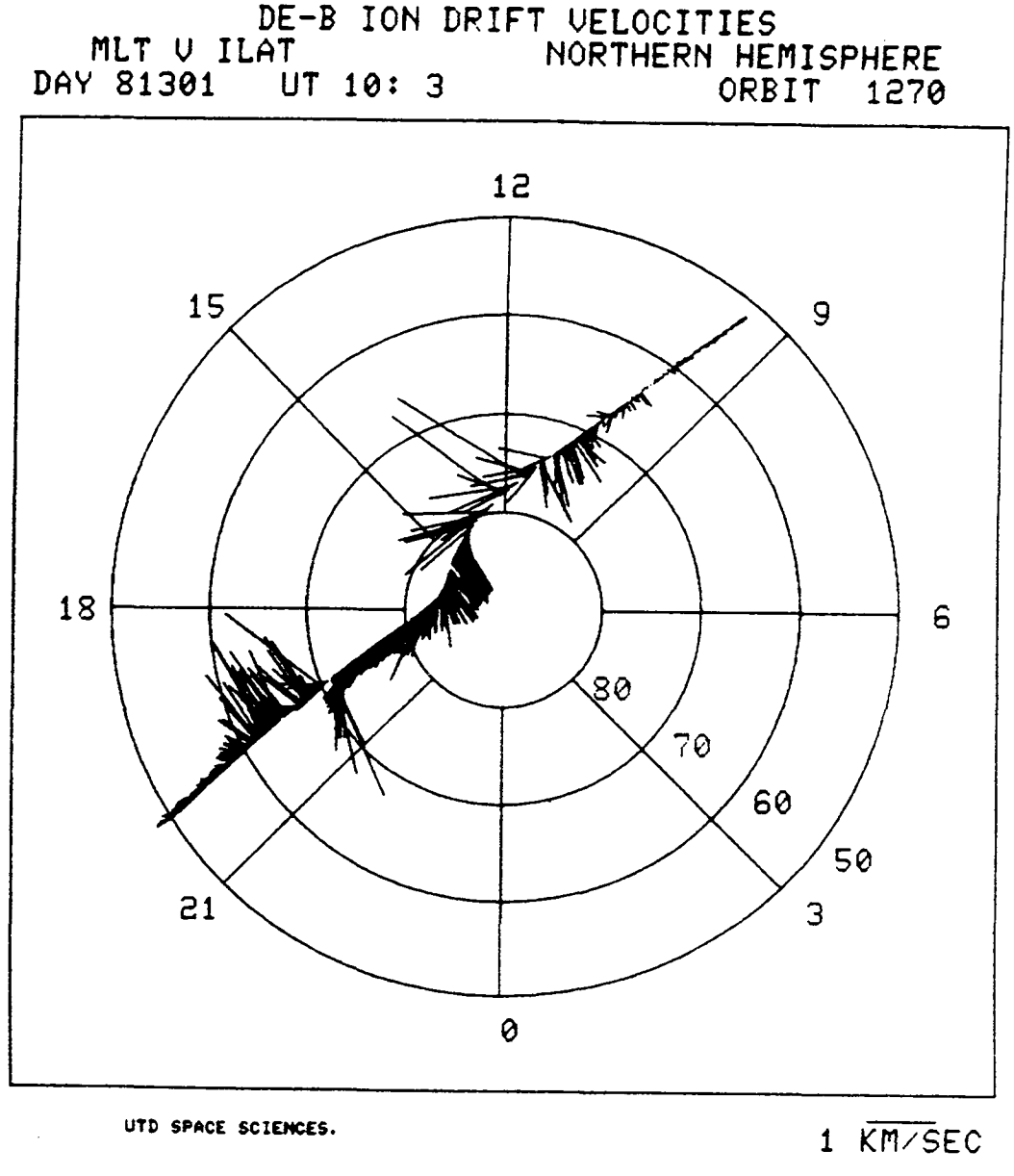
DE-B ION DRIFT VELOCITIES
MLT V ILAT
NORTHERN HEMISPHERE
DAY 81301 UT 10: 3
ORBIT 1270
12
9
6
3
0
21
18
15
80
70
60
50
UTD SPACE SCIENCES.
1 KM/SEC

Figure 5.

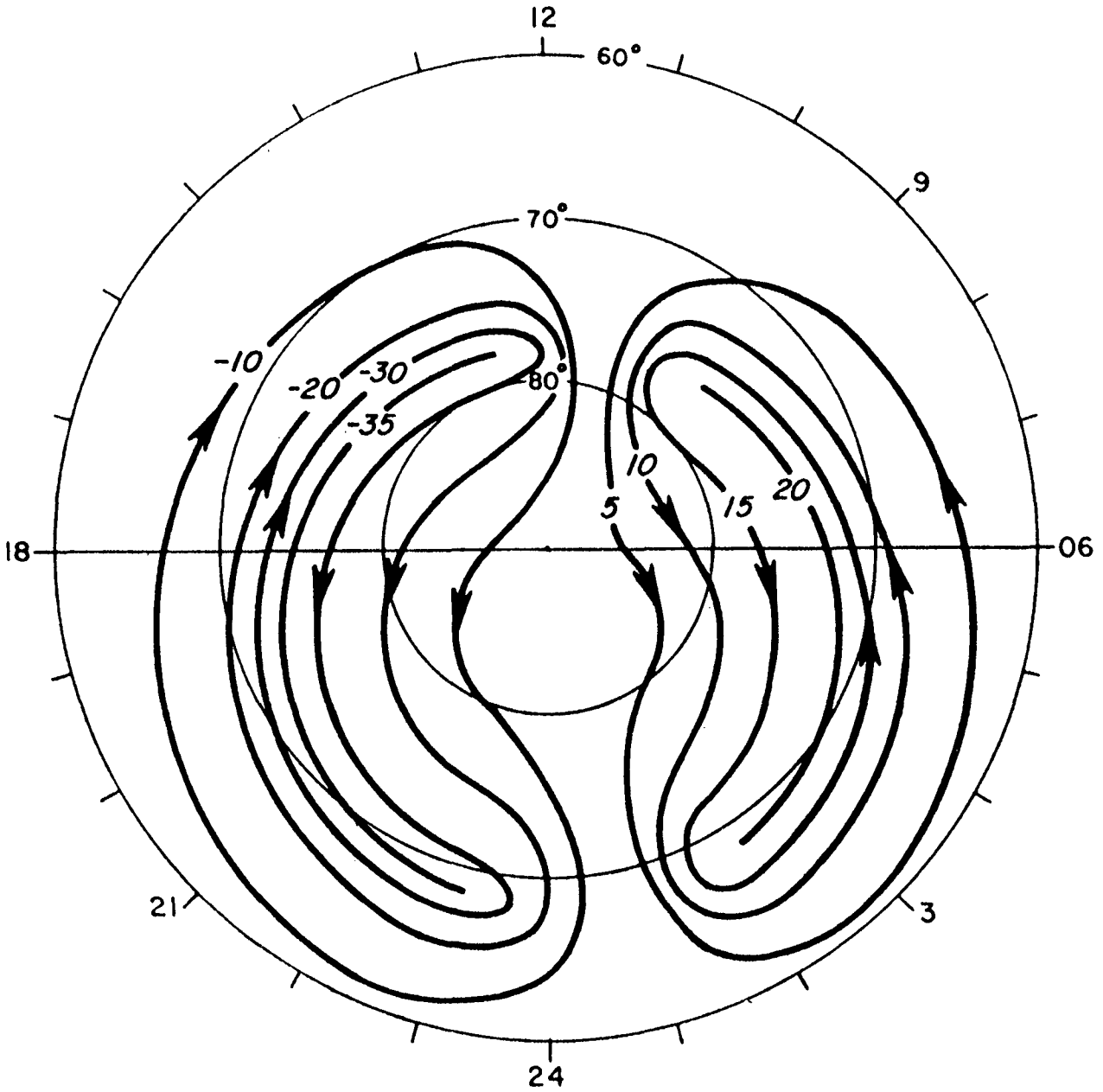

Figure 6.

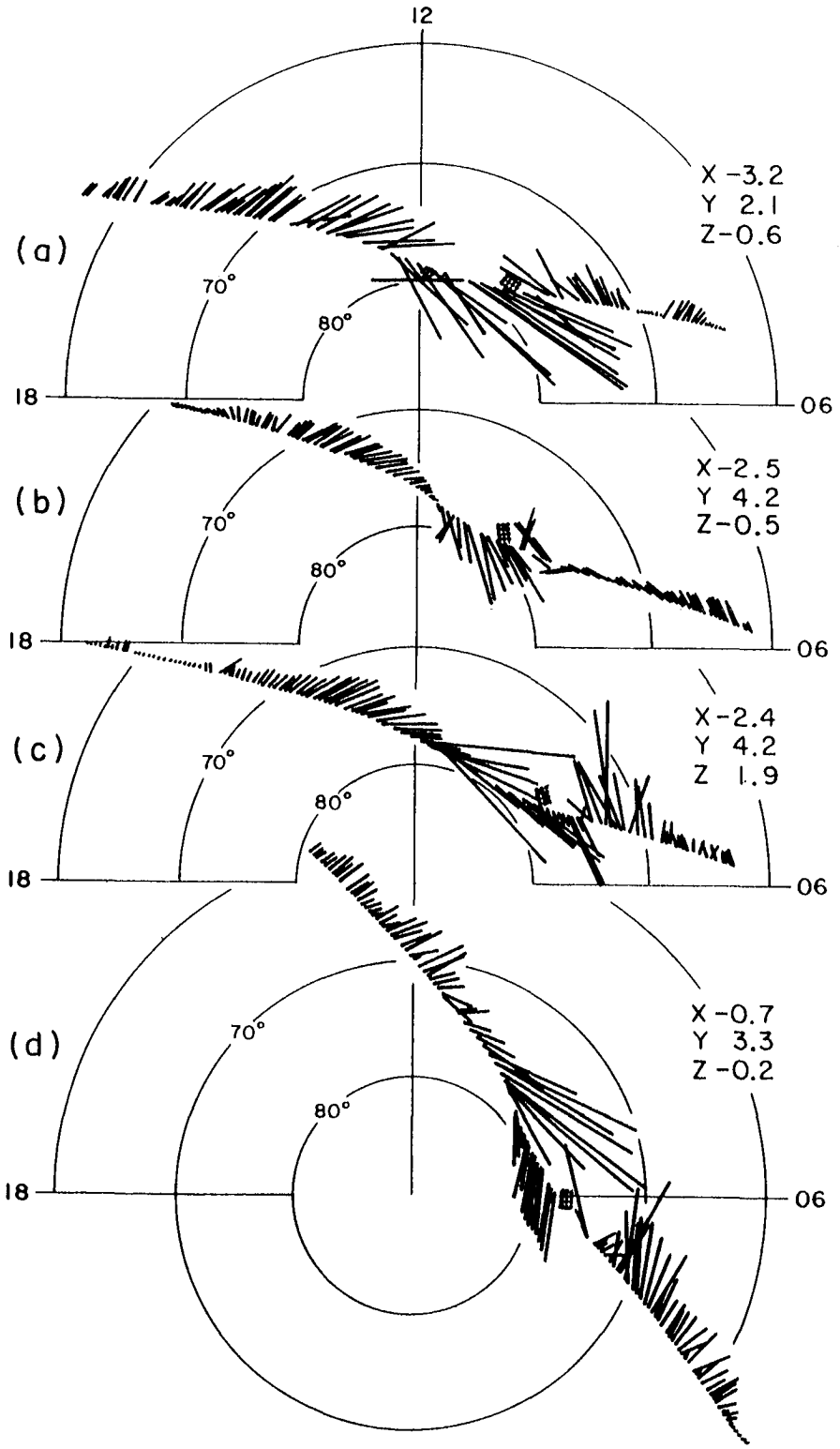
12
(a)
X -3.2
Y 2.1
Z-0.6
70°
80°
18
06
(b)
X-2.5
Y 4.2
Z-0.5
70°
80°
18
06
(c)
X-2.4
Y 4.2
Z 1.9
70°
80°
18
06
(d)
X-0.7
Y 3.3
Z-0.2
70°
80°
18
06

Figure 7.

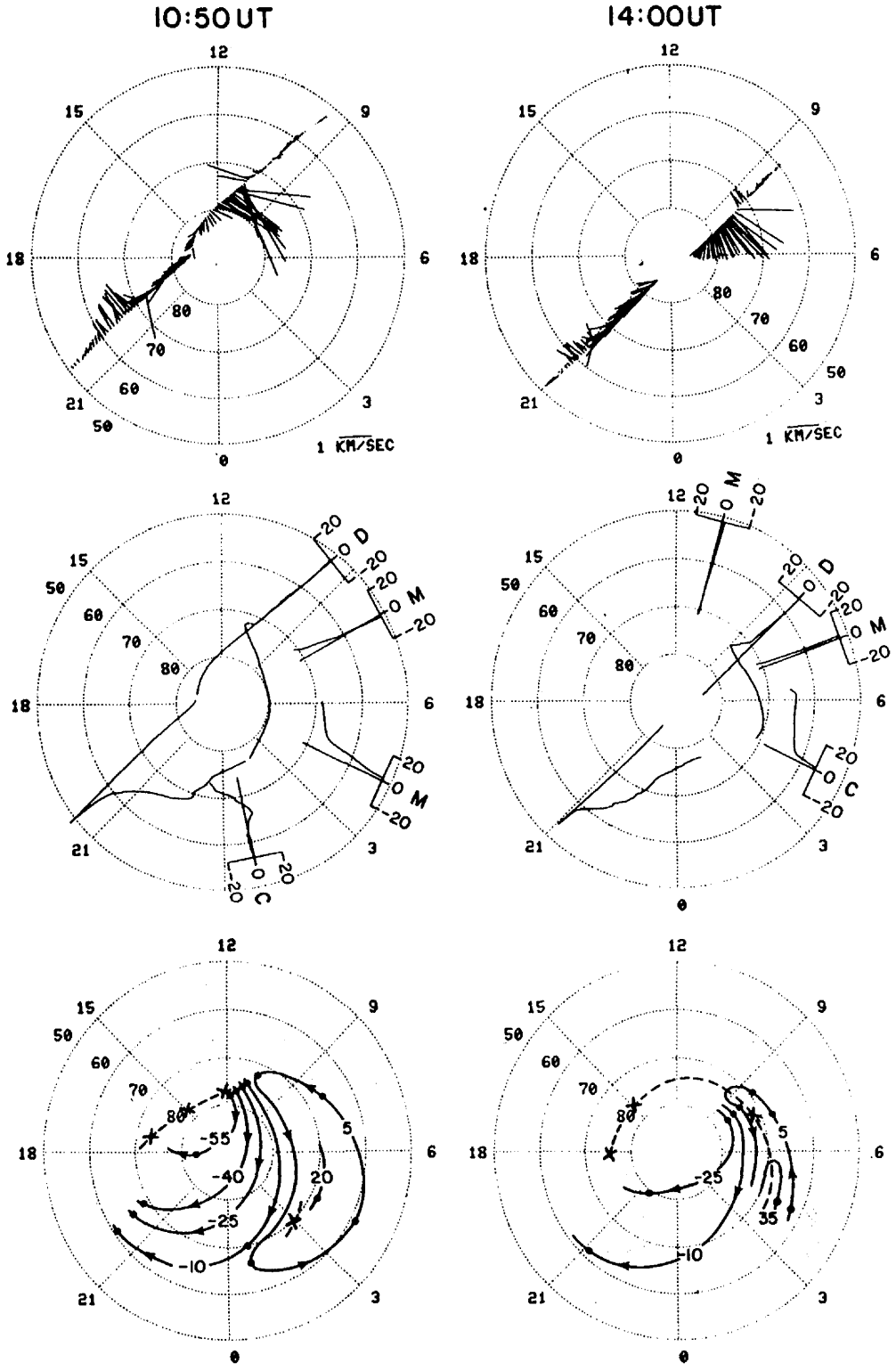

Figure 8.

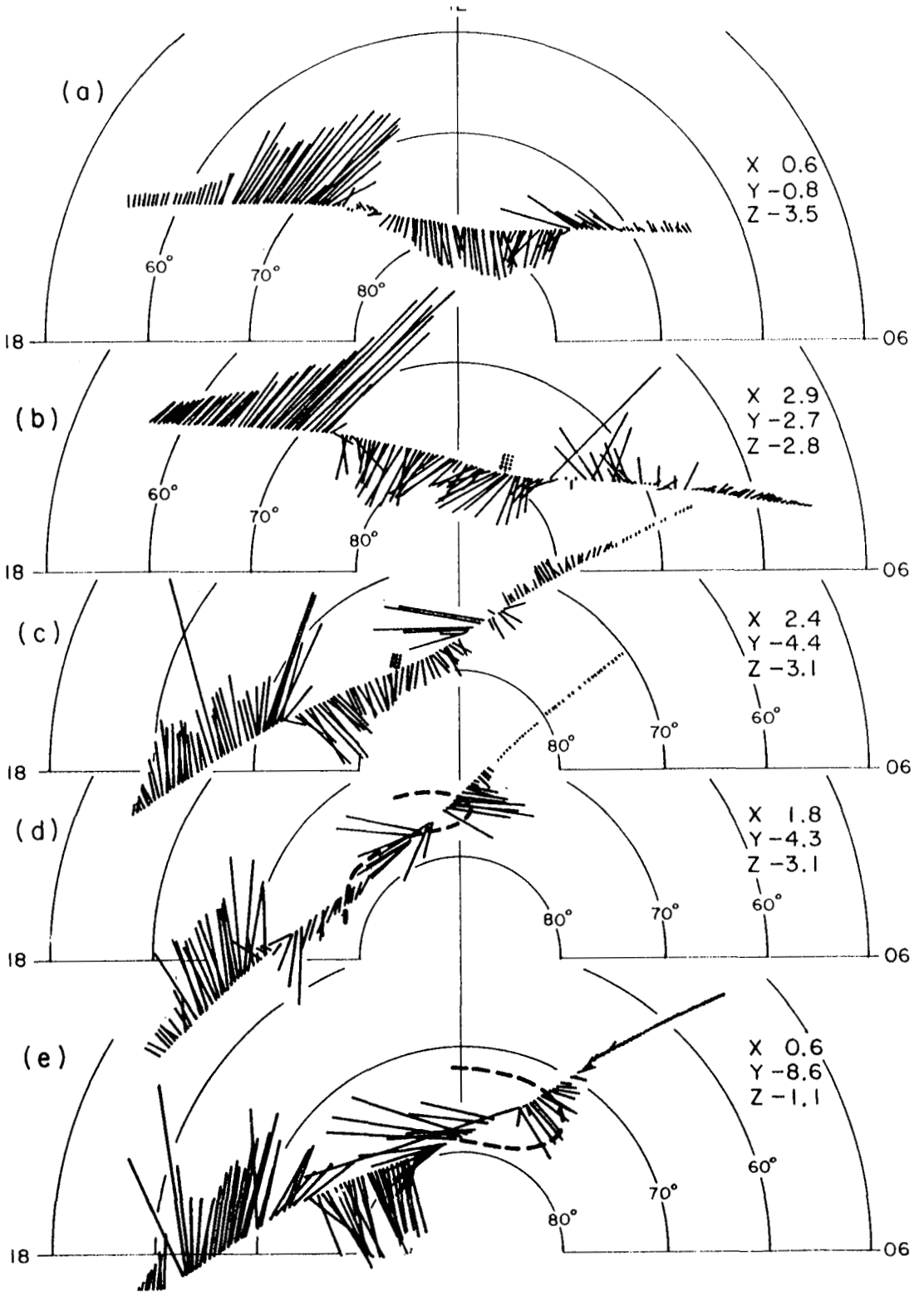
(a)
X 0.6
Y -0.8
Z -3.5
60°
70°
80°
18
06
(b)
X 2.9
Y -2.7
Z -2.8
60°
70°
80°
18
06
(c)
X 2.4
Y -4.4
Z -3.1
60°
70°
80°
18
06
(d)
X 1.8
Y -4.3
Z -3.1
60°
70°
80°
18
06
(e)
X 0.6
Y -8.6
Z -1.1
60°
70°
80°
18
06

Figure 9.

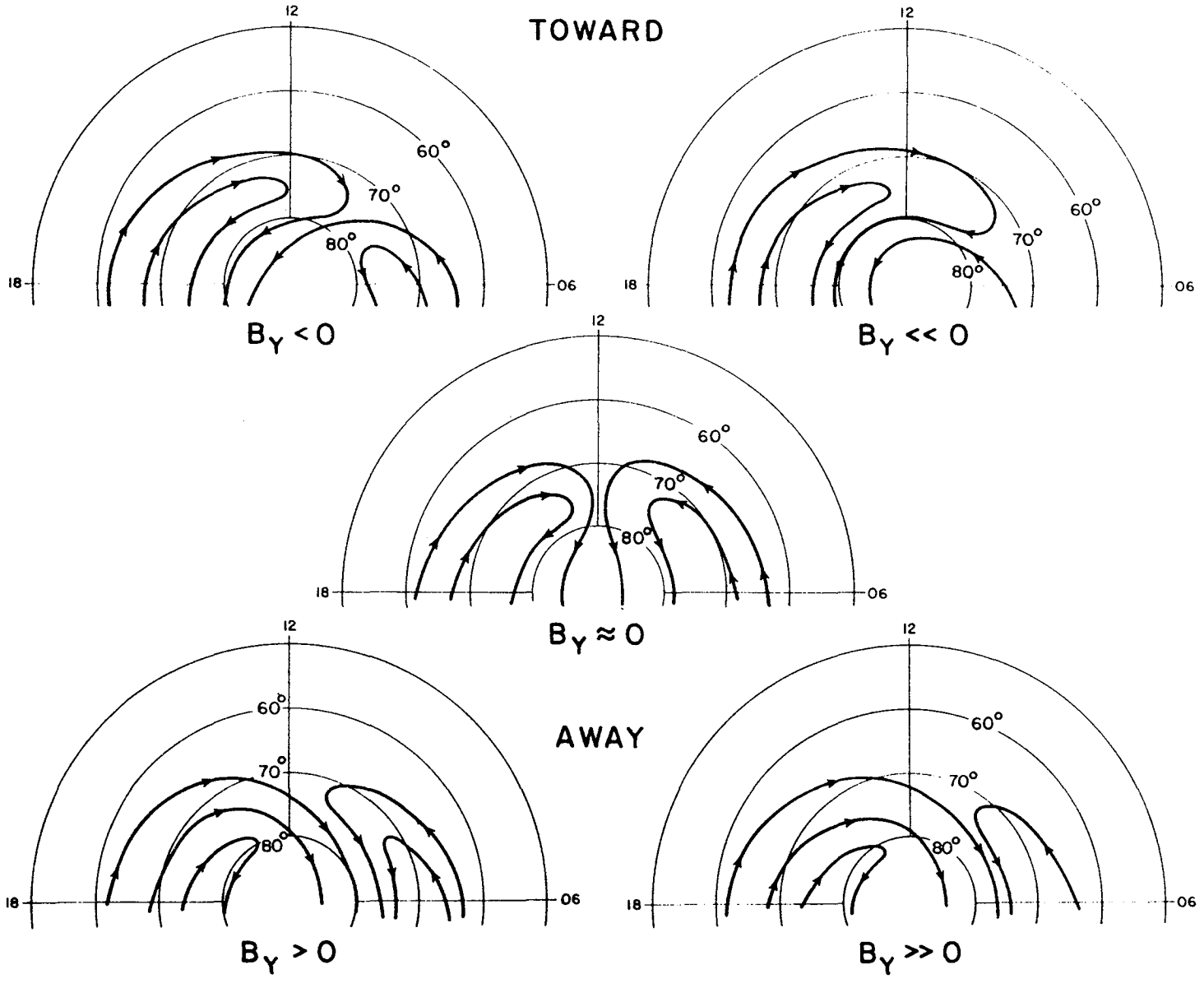

Figure 10.

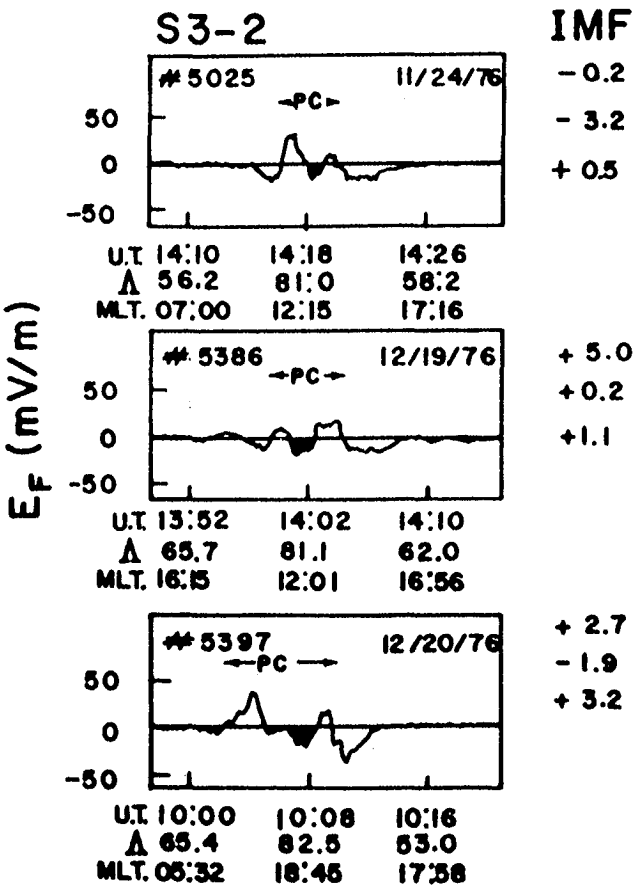
S3-2
IMF
#5025
11/24/76
-PC-
50
0
-50
U.T. 14:10 14:18 14:26
Λ 56.2 81.0 58.2
MLT. 07:00 12:15 17:16
-0.2
-3.2
+0.5
#5386
12/19/76
-PC-
50
0
-50
U.T. 13:52 14:02 14:10
Λ 65.7 81.1 62.0
MLT. 16:15 12:01 16:56
+5.0
+0.2
+1.1
#5397
12/20/76
←PC→
50
0
-50
U.T. 10:00 10:08 10:16
Λ 65.4 82.5 63.0
MLT. 05:32 18:46 17:58
+2.7
-1.9
+3.2
E_F (mV/m)

Figure 11.

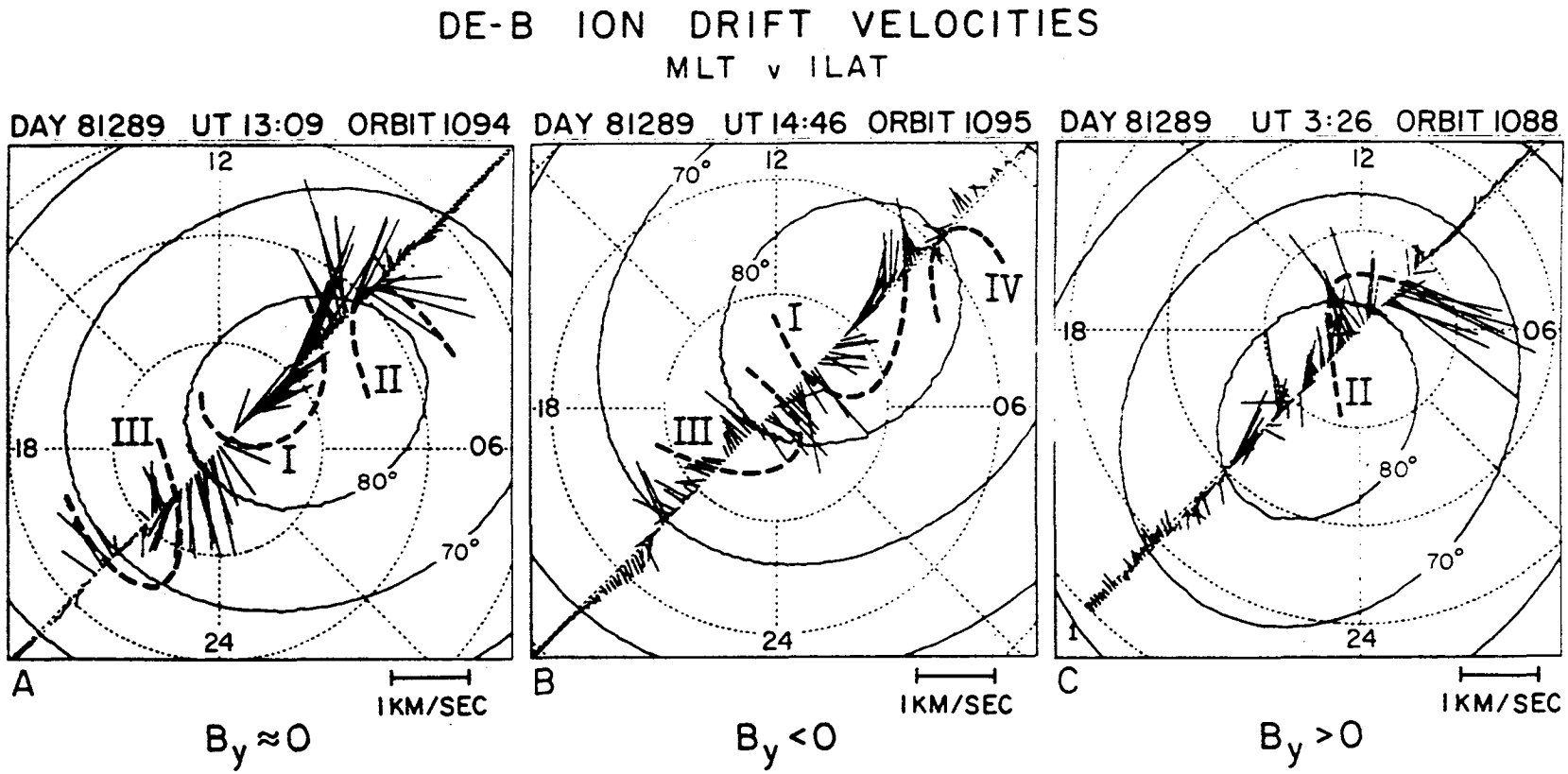
DE-B ION DRIFT VELOCITIES
MLT v ILAT
DAY 81289 UT 13:09 ORBIT 1094
DAY 81289 UT 14:46 ORBIT 1095
DAY 81289 UT 3:26 ORBIT 1088
12
18
06
24
70°
80°
I
II
III
IV
A
B
C
1KM/SEC
By ≈ 0
By < 0
By > 0

Figure 12.

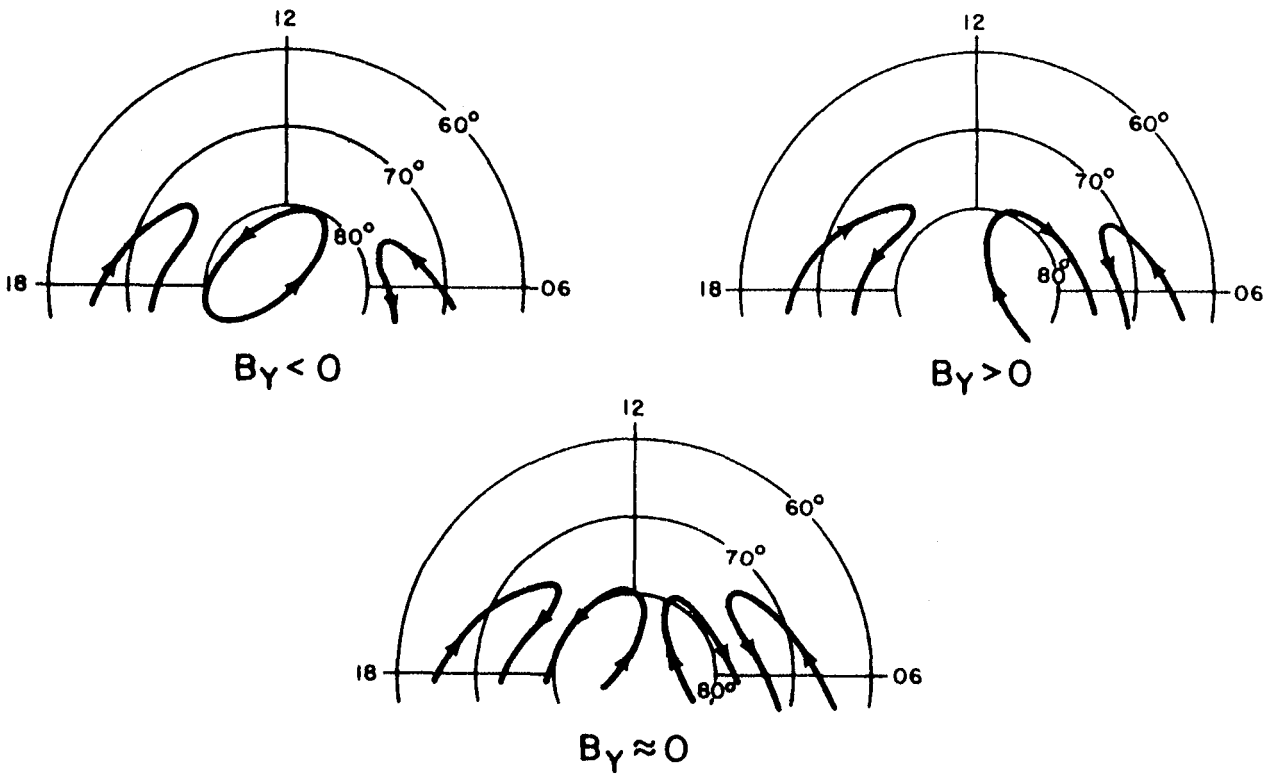
12
60°
70°
80°
18
06
$B_Y < 0$
12
60°
70°
80°
18
06
$B_Y > 0$
12
60°
70°
80°
18
06
$B_Y \approx 0$

Figure 13.